Journal of Atmospheric and Terrestrial Physics, Vol. 48, Nos 9–10, pp. 987–1008, 1986.
Printed in Great Britain.

0021–9169/86 $3.00 + .00
Pergamon Journals Ltd.

A survey of simultaneous observations of the high-latitude ionosphere and interplanetary magnetic field with EISCAT and AMPTE-UKS

D. M. WILLIS, M. LOCKWOOD
Rutherford Appleton Laboratory, Chilton, Didcot, Oxon OX11 0QX, U.K.

S. W. H. COWLEY
Blackett Laboratory, Imperial College, London SW7 2BZ, U.K.

A. P. VAN EYKEN,* B. J. I. BROMAGE, H. RISHBETH
Rutherford Appleton Laboratory, Chilton, Didcot, Oxon OX11 0QX, U.K.

P. R. SMITH†
Blackett Laboratory, Imperial College, London SW7 2BZ, U.K.

and

S. R. CROTHERS
Rutherford Appleton Laboratory, Chilton, Didcot, Oxon OX11 0QX, U.K.

(*Received for publication* 25 *March* 1986)

Abstract—This paper surveys the results of simultaneous observations by the EISCAT incoherent scatter radar and the AMPTE-UKS satellite, made during three periods in September and October 1984, when AMPTE-UKS was in the solar wind on the dayside of the Earth and the UK-POLAR EISCAT experiment was measuring ionospheric parameters at invariant latitudes 70.8–75.0°. A total of 42 h of EISCAT convection velocity data, with 2.5 min resolution, were obtained, together with 28 h of simultaneous 5 s resolution AMPTE-UKS observations of the solar wind and interplanetary magnetic field (IMF). The general features of the AMPTE-UKS data are described in Section 2 and those of the EISCAT data are described in Sections 3 and 4. The main subjects discussed are the form of the plasma convection patterns and their dependence on all three components of the IMF (Section 5), the ionospheric response to abrupt changes in the IMF (Section 6), in particular a sharp 'southward turning' of the IMF on 27 October 1984, and a crossing of an IMF sector boundary. Section 7 describes 'short lived rapid flow bursts', which are believed to be related to flux transfer events at the magnetopause.

1. INTRODUCTION

The patterns of high-latitude *F*-region convection and *E*-region currents are known to depend upon the orientation of the interplanetary magnetic field (IMF) relative to the axis of the Earth's magnetic field (see reviews by COWLEY, 1980; HEELIS, 1982; HEELIS and REIFF, 1985; and references therein). This dependence has been studied using a wide variety of satellite monitors of the interplanetary medium in conjunction with both low-altitude polar-orbiting satellites and ground-based radar and magnetometer observations. Ground-based studies have a major advantage in that a given region can be monitored continuously. This provides information on the temporal evolution of the currents and plasma motions in response to IMF changes, not just snapshots as given by satellites. Remote ground-based observations, however, cannot achieve the accuracy or resolution of *in situ* observations by satellites. This has led to combined studies using several ground-based systems and simultaneous satellite data (e.g. HEELIS *et al.*, 1983).

The present study takes advantage of the special opportunity of monitoring the IMF, just outside the bow shock, presented by the AMPTE mission (BRYANT *et al.*, 1985). The UKS satellite carried a fluxgate magnetometer (SOUTHWOOD *et al.*, 1985) and

*Present address: Millstone Hill Radar, M.I.T.-Haystack Observatory, Westford, MA 01886, U.S.A.
†Present address: University College London, Gower St., London WC1E 6BT, U.K.

followed an elliptical orbit with apogee at 18.7 R_E (Earth radii). Hence the delay time between features in the interplanetary field being observed by the spacecraft and arriving at the Earth's magnetopause can be estimated more accurately than from a satellite in orbit around an Earth–Sun libration point (such as ISEE 3 near 250 R_E). The reception of data from UKS in real time at the Rutherford Appleton Laboratory facilitated experiment planning, in particular by defining when UKS was in the solar wind upstream of the bow shock.

The plasma convection pattern is studied with high time resolution by the EISCAT radar, using the UK Special Programme POLAR, which produces velocity vectors with 2.5 min resolution at invariant latitudes 70.8–75.0°. The Sondrestrom radar has also been used to study IMF effects on convection (CLAUER *et al.*, 1984) over the range 70–80°; this range is observed in a cycle time of 27 min and is divided into 5 subranges for which vectors are derived in a 5 min beam-swinging period. Hence, the EISCAT data cover a smaller range of latitudes, but with higher time resolution.

From the studies described above, the pattern of plasma convection is known to vary greatly with the north–south component of the IMF (B_z). If the IMF has a large southward component ($B_z < 0$), the convection pattern is generally large and two-celled (CAUFFMAN and GURNETT, 1972; HEPPNER, 1972). The observed pattern of flow might, in principle, arise from either a viscous-like interaction at the magnetopause or from field line merging at the dayside magnetopause. Initial studies of the variation of the cross-cap potential driving this convection pattern showed that only 30 kV were generated by a viscous-like interaction, but that magnetic merging gave up to about 150 kV, depending on the orientation of the IMF (REIFF *et al.*, 1981). Subsequent analysis has shown that most of this apparent viscous interaction arises from the residual effect of magnetic merging, which takes several hours to decay (WYGANT *et al.*, 1983), and the viscous interaction gives at most 10–20 kV (MOZER, 1984; COWLEY, 1986). The two-cell pattern for southward IMF is distorted by the dawn–dusk B_y component of the IMF, the major effect of B_y being to introduce a dawn–dusk component into the anti-sunward flow in the polar cap (HEELIS, 1984), an effect which arises as a natural consequence of field line tension for a merging model (JØRGENSEN *et al.*, 1972; COWLEY, 1980).

When the northward component of the IMF B_z is positive, convection is generally much slower and confined to higher invariant latitudes (e.g. FRIIS-CHRISTENSEN *et al.*, 1985). The pattern of flow is much more irregular on the nightside and in the winter hemisphere (HEPPNER, 1972; HEELIS and HANSON, 1980). The major change on the dayside from the southward IMF case is that a region of sunward flow is found within the polar cap (MAEZAWA, 1976; BURKE *et al.*, 1979; ZANETTI *et al.*, 1984; HEELIS, 1986). As in the case of southward IMF, the B_y component of the IMF affects the pattern of flow giving dawn–dusk asymmetries within the cap; the convection pattern has three cells when the magnitude of B_y is large and four cells when B_y is close to zero. The additional one or two convection cells in the polar cap can be attributed to merging between the northward IMF and geomagnetic field, which are adjacent and anti-parallel at the cusps (e.g. REIFF, 1982).

These studies have shown how field line merging, with a small contribution from a viscous-like interaction, can explain the variety of convection patterns observed for different stable orientations of the IMF (BURCH and REIFF, 1985; REIFF and BURCH, 1985; BURCH *et al.*, 1985). For the reasons outlined at the beginning of this Introduction, the temporal evolution of the convection pattern in response to changes in the IMF is not well known. Following a northward turning of the IMF, a large amount of geomagnetic flux remains 'open', i.e. connected to the IMF, and hence continues to drive convection. As these open flux tubes move tailward and reconnect in the plasma sheet, the convection slowly decays, as observed by WYGANT *et al.* (1983). A contracted convection pattern is only observed when the IMF is consistently northward for at least 2 or 3 h. However, when the IMF turns southward, the rate at which geomagnetic flux can be connected to the IMF depends on the value of B_z and is much greater than the rate by which open flux is lost following a northward turning. Hence, an enhanced, expanded pattern typical of southward IMF should be established much more rapidly than it decays. NISHIDA (1968) noted that the DP2 current system, thought to be the current signature of polar convection, was enhanced at high latitudes 7 ± 1 min after a southward turning of the IMF impinged upon the Earth's bow shock. Similar delays have been reported recently from data from CDAW6 (Combined Data Analysis Workshop) studies (MCPHERRON and MANKA, 1985; CLAUER and KAMIDE, 1985), but have never been explained.

Changes in convection in response to IMF changes have been reported by CLAUER *et al.* (1984) and CLAUER and BANKS (1986) from Sondrestrom incoherent scatter radar data of 25 min resolution. Part of the EISCAT data set described in the present paper has been used to quantify the lag with which the convection pattern responds to a southward turning

of the IMF at the magnetopause (RISHBETH *et al.*, 1985). LOCKWOOD *et al.* (1986) have shown that the observed lag is consistent with the rate of expansion of the new, enhanced pattern and the rate at which flux can be connected at the dayside magnetopause.

In addition to changes in steady reconnection rates brought about by changes in the IMF, short lived bursts of reconnection, called flux transfer events (FTEs), have been observed at the magnetopause (HAERENDEL *et al.*, 1978; RUSSELL and ELPHIC, 1978). Theoretical predictions of the form of the signature of FTEs in the ionosphere (SOUTHWOOD, 1984) predict a small, short lived, twin vortex flow pattern with rapid poleward flow in the centre. Bursts of rapid poleward flow have been observed by both the EISCAT (VAN EYKEN *et al.*, 1984) and STARE (GOERTZ *et al.*, 1985) radars. Further examples of such bursts are presented in Section 7 of this paper, along with a discussion of their implications for our understanding of magnetopause phenomena.

2. AMPTE OBSERVATIONS

The dashed line in Fig. 1 shows the elliptical orbit of the AMPTE-UKS satellite shortly after its launch on 16 August 1984. The locations of the apogee (at 18.7 R_E) in the X–Y plane of the GSM coordinate system are shown for various days during the mission, which lasted until 15 January 1985. The solid and open points in Fig. 1 show, respectively, the locations of the magnetopause and of the bow shock, as observed by UKS using the energy–time spectrograms from the three-dimensional ion (COATES *et al.*, 1985) and electron (SHAH *et al.*, 1985) experiments. Full instrument and calibration details have been given by SOUTHWOOD *et al.* (1985) and COATES *et al.* (1985) for the magnetometer and ion experiment, respectively. The three short curves in Fig. 1 show sections of three orbits during which the magnetometer on UKS observed the IMF in the solar wind, upstream of the bow shock and near the Sun–Earth line ($Y = 0$), and simultaneous observations of ionospheric convection were made by EISCAT (see Table 1). The satellite is well sunward of the normal locations of the bow shock during the whole of these three periods and the ion flow data show that the flows have not been slowed nor thermalised by the bow shock. Hence, the magnetometer and the ion experiment were observing the interplanetary medium shortly before it impinged upon the Earth's bow shock.

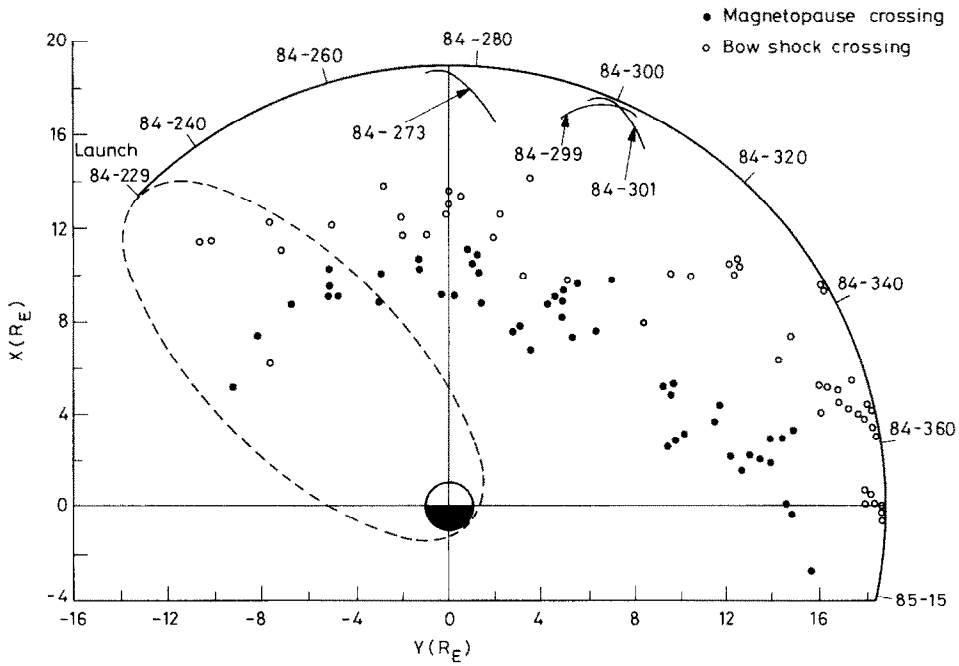

Fig. 1. Locations of magnetopause (solid circles) and bow shock (open circles) crossings observed by the AMPTE-UKS satellite in the X–Y plane of the GSM coordinate system. The dashed line shows the initial orbit of UKS and the dates give the locations of satellite apogee during its life-time. The short solid curves show the locations of the satellite during the periods of simultaneous observations with the EISCAT radar, as listed in Table 1.

Table 1. Periods of EISCAT and UKS observations

Date	Day no.	Time of AMPTE observations UT	Time of EISCAT observations UT	Time of EISCAT observations MLT	*Kp* sum	*Ap*	$F_{10.7}$
29 Sept 1984	273	0710–1650	0726–1756	0954–2029	20+	12	72
25 Oct 1984	299	0545–1520	2313–1523*	0127–1803	27	22	70
27 Oct 1984	301	0605–1510	2348–1530*	0201–1808	16+	8	69

*Observations commenced on the previous day.

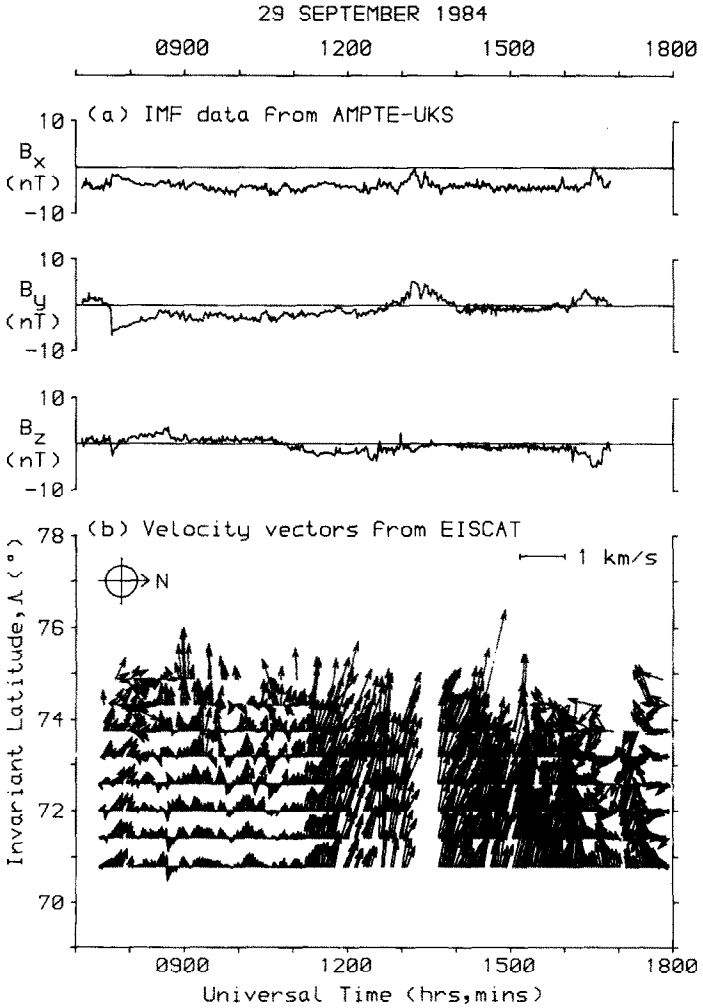

Fig. 2. (a) One minute integrations of the three components of the IMF, in the GSM frame, observed by UKS. (b) the 2.5 min resolution EISCAT velocity vectors observed simultaneously shown as a function of Universal Time (UT). 29 September 1984.

The first three panels of Figs. 2–4 show the three components of the IMF in the GSM frame of reference, observed by AMPTE-UKS during the three periods. These values have been integrated over 1 min periods to smooth out rapid fluctuations due to upstream waves (5 s data are shown for limited periods in Figs. 9 and 11). On 29 September the IMF is relatively steady, with negative B_x, mainly small B_z and with B_y changing from negative to positive to near zero. The IMF shows even less variation on 25 October, with slightly negative B_z, positive B_y and negative B_x. On 27 October, however, there is considerably greater fluctuation in the IMF. From 0800 UT the IMF was northward for over 3 h, until the abrupt southward turning at 1107 UT. In addition, both B_y and B_x turn from negative to positive at 1238 UT, indicating that an IMF sector boundary passed over the spacecraft.

3. EISCAT OBSERVATIONS

The UHF Special Programme UK-POLAR has been described by van Eyken *et al.* (1984). Signals are transmitted and received at Tromsø, at elevation 21.5°, alternately in geographic azimuths 332° and 356°. Since the mean direction (344°) is approximately the L-shell meridian at Tromsø, a pair of points at equal ranges in the two directions are at practically

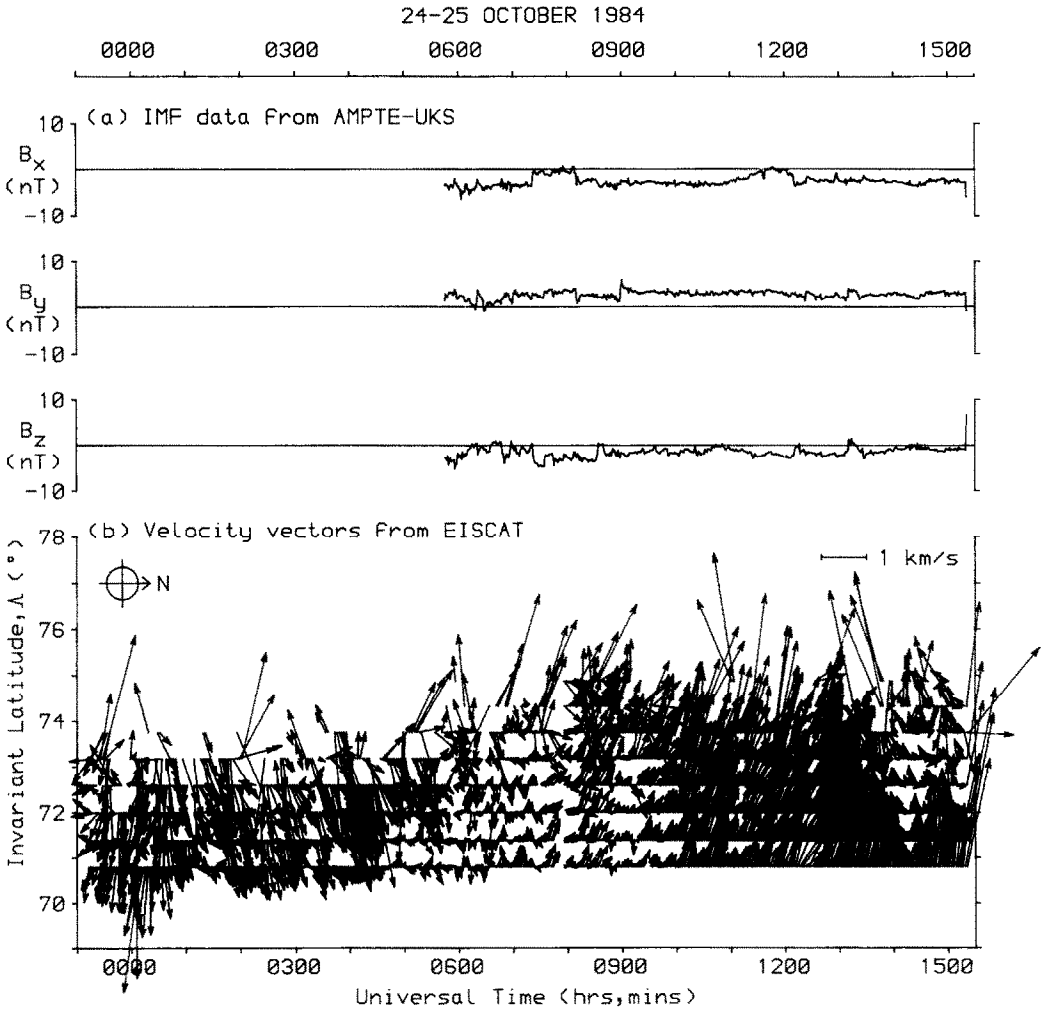

Fig. 3. As Fig. 2, but for 24–25 October 1984.

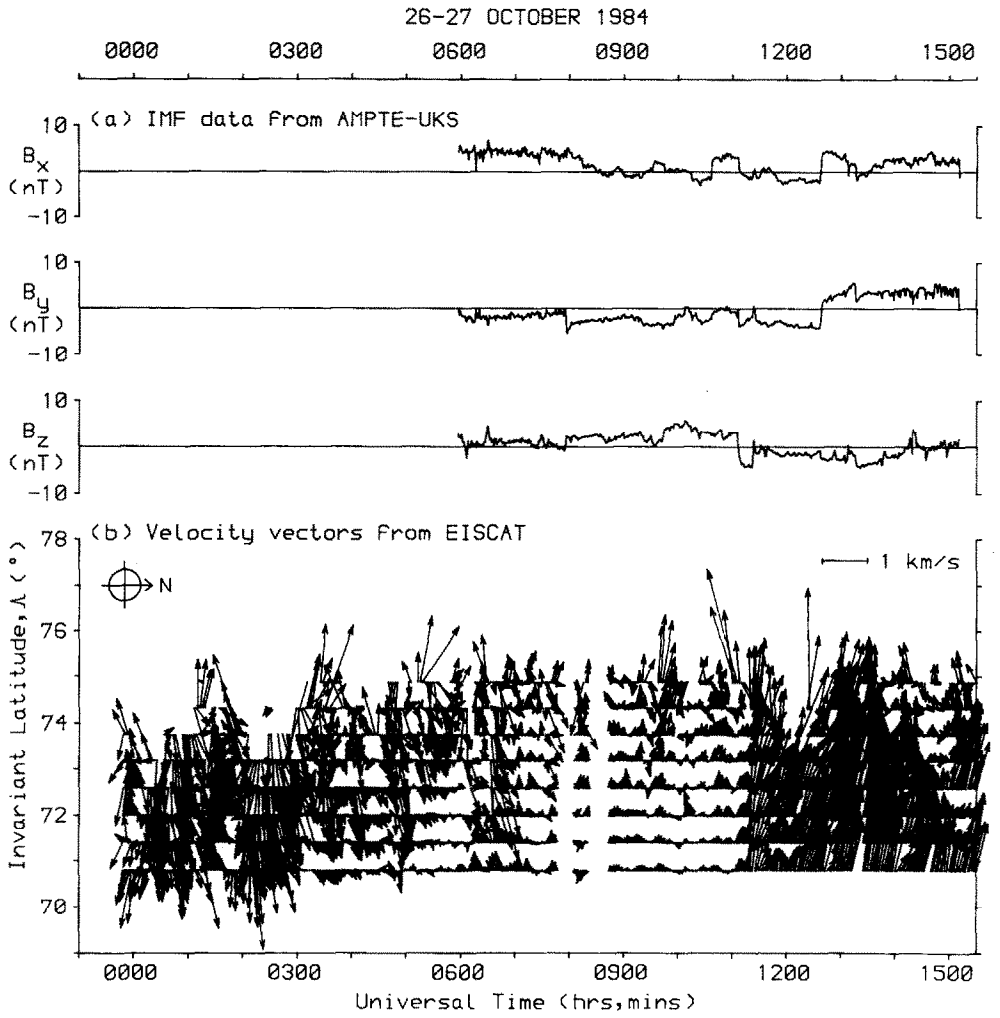

Fig. 4. As Fig. 2, but for 26–27 October 1984.

the same invariant latitude (see fig. 2 of VAN EYKEN *et al.*, 1984). The basic assumptions made by van Eyken *et al.* are that the northward and eastward components of the plasma velocity at any such pair of points is the same and that it remains constant during the beam-swinging cycle, so that the line-of-sight velocities may be combined to give two components of the vector velocity at the midpoint of the pair. For the beam directions described above, the assumption of spatial uniformity is made over a distance of 218 km for the range gates at 70.8° invariant latitude, increasing to 436 km for those at 75.0°. Given that only two measurements are made of the three-dimensional velocity vector, a necessary further assumption is that the field-aligned component is negligible. The geometry of the POLAR experiment is such that an appreciable field-aligned velocity (say 50 m s^{-1}) would in general make little difference to the results.

The procedure used in this paper is essentially the same as in the previous paper, but improvements in the efficiency of the experiment have made it possible to reduce the dwell time at each pointing direction from 4.5 to 2 min, thereby halving the total cycle time. In addition, a slightly different assumption about the temporal behaviour of the velocities is made: the line-of-sight components in each direction are linearly interpolated between the adjacent values 5 min apart. Hence, every 2.5 min a measured line-of-sight velocity for one azimuth is combined with an interpolated

value for the other azimuth. Expressions for the accuracy in direction and magnitude of the velocity vectors determined from the POLAR data are derived in the Appendix, which also includes a discussion of the dependence of the accuracy on the direction and magnitude of the flow. The experiment uses 0.5 ms pulses and 75 km non-overlapping range gates. The data presented in this paper are for gates 1–8 at ranges 525(75)1050 km, at invariant latitudes 70.8(0.6)75.0° and at heights ranging from 211 km for gate 1 to 455 km for gate 8. A satisfactory signal-to-noise ratio, expressed as (signal)/(background) > 0.8%, could usually be obtained in these 8 gates.

To cover the three AMPTE-UKS observing periods, the UK-POLAR experiment was run for the periods given in Table 1. All magnetic local times (MLT) quoted in this paper are computed using an Earth-centred dipole approximation to the geomagnetic field. At a given UT, MLT varies with gate number and pointing direction; the values given above are for the centre of the EISCAT field of view, for which MLT $\simeq$ UT + 2.5 h.

4. EISCAT DATA

Figures 2–4 also show plasma convection velocities for the three periods of EISCAT observations, plotted as a function of UT. The velocities are plotted in a format in which westward plasma flow (produced by northward electric field) is represented by upward pointing arrows, and northward plasma flow (produced by an eastward electric field) is represented by arrows pointing to the right. With the prevailing east–west flows, the diagrams are much less congested than if they were drawn more conventionally, with upward pointing arrows denoting northward flow.

Figures 5–7 give a different representation of the EISCAT data recorded on these three days. The general format of these figures is an invariant latitude (Λ)–magnetic local time (MLT) polar dial representation of field-perpendicular convection vectors **V**, electron density N_e and electron and ion temperatures T_e and T_i. For all parameters the invariant pole ($\Lambda = 90°$) is at the centre of the plot, but the invariant latitude scale is different for each, such that the results appear as concentric circular bands with latitude and gate number increasing inwards. Because data are taken along the slanting beam direction, a height (h) scale is also shown for each band of data. Local magnetic noon is at the top of each polar dial plot, dawn to the right and dusk to the left, so that westward flow is clockwise and eastward flow is anticlockwise on the dials.

The velocity vectors shown in the outer band are 10 min averages of the 2.5 min resolution data obtained by the beam-swinging technique. The averaging allows the general pattern of convection to be seen with greater clarity, but smooths out the considerable small-scale structure seen at higher time resolution (see Sections 6 and 7). The scalar parameters N_e, T_e and T_i shown in Figs. 5–7 are those observed with the antenna pointing in azimuth 332°, for which the MLT is approximately independent of range and hence invariant latitude. In general, the corresponding plots for azimuth 356° are very similar, though there are small but significant differences which are discussed by Lockwood *et al.* (1986). Considerable differences exist between the patterns of convection observed on these three days: in the following subsections all three patterns are discussed, starting with the simplest, namely that of 24–25 October.

4a. *EISCAT data for 24–25 October 1984*

The velocity vectors in Fig. 6 show a relatively weak dawn convection cell in the POLAR field of view. After 0600 MLT, the region of eastward flow is only observed in the further range gates at the higher invariant latitudes, where lower signal-to-noise ratios of the data also give greater scatter in the velocities. By comparison, the dusk cell is relatively strong and regular, with westward flows seen at all MLT after 1000. The flows tend to turn increasingly northward as they reach earlier MLT. The flow pattern is consistent with a throat (see Section 5a) near 1000 MLT. After about 1615 MLT, consistent westward flows are only seen in the first two range gates; it is possible that the further gates are observing a region of low convection inside the polar cap.

The plasma densities are very low throughout the observed part of the dawn cell and larger values are not observed until the dusk cell moves into the radar field of view. The higher densities near noon are qualitatively consistent with enhancement by solar photoionization, which extends into the morning sector only as far as the throat, whence enhanced densities would be swept into the polar cap. Note that the general decrease in topside density beyond gate 3 is due to the increasing height of the observations. In the afternoon sector the field of view sweeps through a broad depletion which coincides with the band of fast westward convection and is therefore consistent with the extension of the mid-latitude trough towards noon, as reported by Evans *et al.* (1983) and Lockwood *et al.* (1984).

The other interesting features in Fig. 6 are the bands of enhanced ion temperature which sweep across the

POLAR field of view near 0600 and 1400 MLT. In the afternoon sector, the high ion temperatures appear at the higher invariant latitudes and move equatorward with increasing MLT; they coincide with the low plasma densities and the high convection speeds. In the dawn sector the apparent motion of the high ion temperatures is poleward. If the ion heating is ascribed to ion–neutral friction, then the ion temperature data effectively image the auroral and subauroral return flows of the convection pattern.

4b. *EISCAT data for 26–27 October 1984*

The convection velocities observed near noon on this day (shown in Fig. 7) are considerably smaller than for two days earlier, a consistent, strong dusk convection cell not being apparent until a sudden increase in westward flow is seen in all range gates near 1400 MLT (see also RISHBETH *et al.*, 1985; LOCKWOOD *et al.*, 1986). As on 25 October, the dawn cell is weak after 0600 MLT, but shows several short lived enhancements. The higher plasma density at noon on this day may be a consequence of the slower convection speed, which allows the sunlight-produced ionization to build up, instead of being moved away. The densities observed in the morning sector and near dusk are also higher and the trough seen in the afternoon sector is narrower than on 25 October. The bands of enhanced ion temperature are again observed, this time coinciding with elevated electron temperatures and lying slightly poleward of the trough. The enhancement in convection speeds near 1400 MLT is accompanied by a brief rise and subsequent fall in ion temperature, seen in all range gates simultaneously; this is attributed to ion–neutral frictional heating (Section 6a).

4c. *EISCAT data for 29 September 1984*

Data for the shorter run on 29 September are shown in Fig. 5. Convection speeds are again generally low near noon, with a more gradual enhancement in westward flow seen near 1400 MLT. As for 25 October, a rise and fall in ion temperature is seen at this time. Subsequently, strong and consistent westward flows are observed until 1900 MLT, when they turn southward, suggesting that the field of view is approaching the Harang discontinuity. On this day no trough is seen in the afternoon sector and the band of ion temperature enhancement is much weaker; both of these features may be due to the smaller zenith angle of solar illumination than for October. The electron temperature is also consistently higher on this day.

5. DEPENDENCE OF CONVECTION ON THE IMF

5a. *Differences in the patterns of convection for different steady orientations of the IMF*

As discussed in the Introduction, the B_z component of the IMF is known to control the strength of convection at all latitudes. However, it is not clear if the B_y effect seen in the polar cap is also seen on closed auroral and subauroral field lines. HEELIS (1984) reports a narrow constricted region of flow into the polar cap, termed the throat, which is always in the pre-noon sector, irrespective of the sense of B_y. It has often been suggested (e.g. FAIRFIELD *et al.*, 1977) that the location of the throat changes with the B_y component of the IMF. However, PRIMDAHL *et al.* (1980, 1981) find that the slant-E condition on ionograms, which they associated with the throat region, is statistically at the same MLT for all B_y values. More direct observations of the region of flow into the polar cap by the Sondrestrom incoherent scatter radar have not revealed a restricted throat such as reported from satellite data (JØRGENSEN *et al.*, 1984). A recent model by REIFF and BURCH (1985) predicts that the merging geometry is such that the convection pattern will depend critically on both B_y and B_x if B_z is small. Another mechanism by which B_y and B_x affect the sub-auroral return flows, even if B_z is strongly negative, is by their effect on the location of the polar cap (COWLEY *et al.*, 1980; MOSES *et al.*, 1985). For example, a large and negative B_y can displace the polar cap and the entire convection pattern towards dusk.

The convection pattern on 24–25 October shows a stagnation region in the dusk sector at the higher invariant latitudes. In order to understand this in terms of a convection pattern with one circular and one crescent-shaped cell, the dusk cell must be circular, which is consistent with the positive B_y on this day. A similar feature is seen at this MLT on 27 October, when B_y was again positive. However, on 29 September it was absent, with strong westward flows persisting at all observed invariant latitudes until after 1800 MLT; during this period B_y was near zero. On all three days the weak dawn cell and the strong dusk cell suggest that the entire pattern is displaced towards dusk. This is a feature which is commonly, but not invariably, observed in EISCAT data from POLAR and other experiments (FARMER *et al.*, 1984; LOCKWOOD *et al.*, 1984), but not in data from other radars further west (e.g. JØRGENSEN *et al.*, 1984). It is therefore possible that these data reflect a longitudinal (and therefore UT) effect on the convection pattern due to the offset of the geomagnetic and rotational poles.

Near noon the polar cap boundary is to the north of the field of view and it is not possible to determine

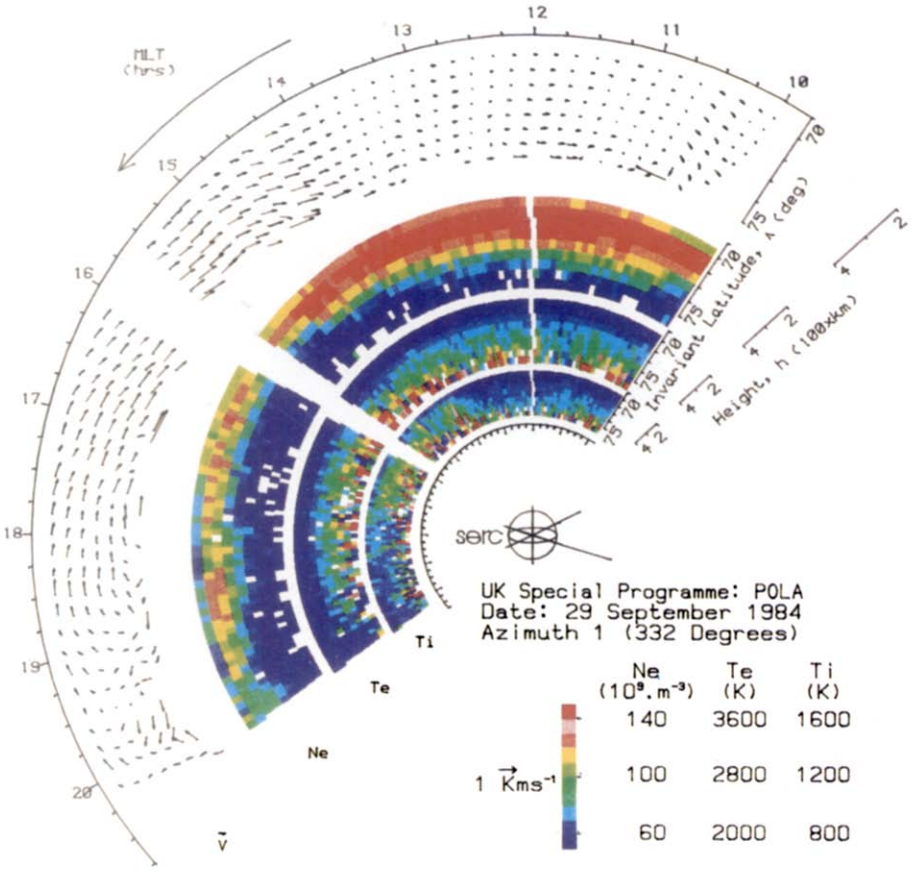

Fig. 5. Polar dial plots of EISCAT data on 29 September 1984, consisting of concentric invariant latitude–MLT plots of 10 min averages of velocity vectors **V**, plasma density N_e, electron temperature T_e and ion temperature T_i. The invariant pole is at the centre of each plot, but the invariant latitude scale is different for each. The corresponding heights of the observations h are also shown. The scalar data are for azimuth 332° only.

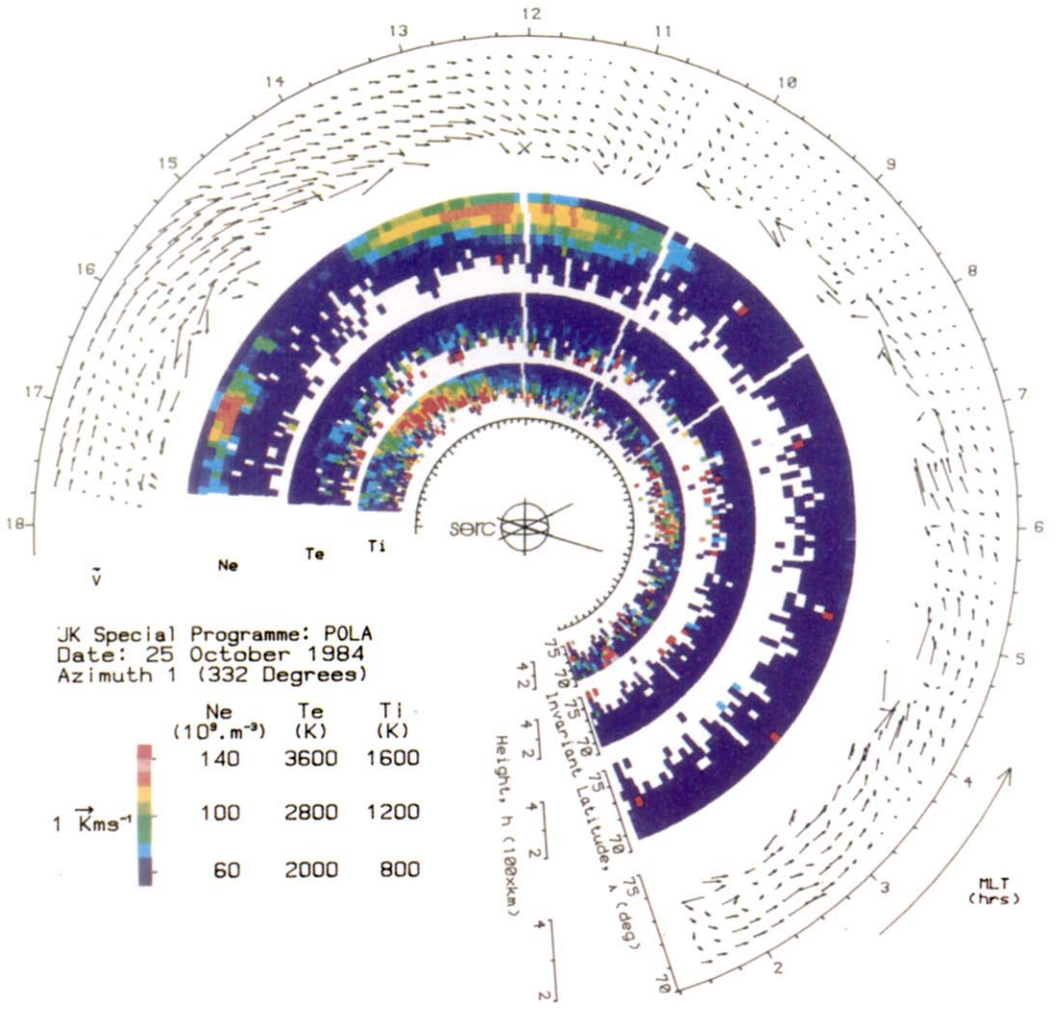

Fig. 6. As Fig. 5, but for 24–25 October 1984.

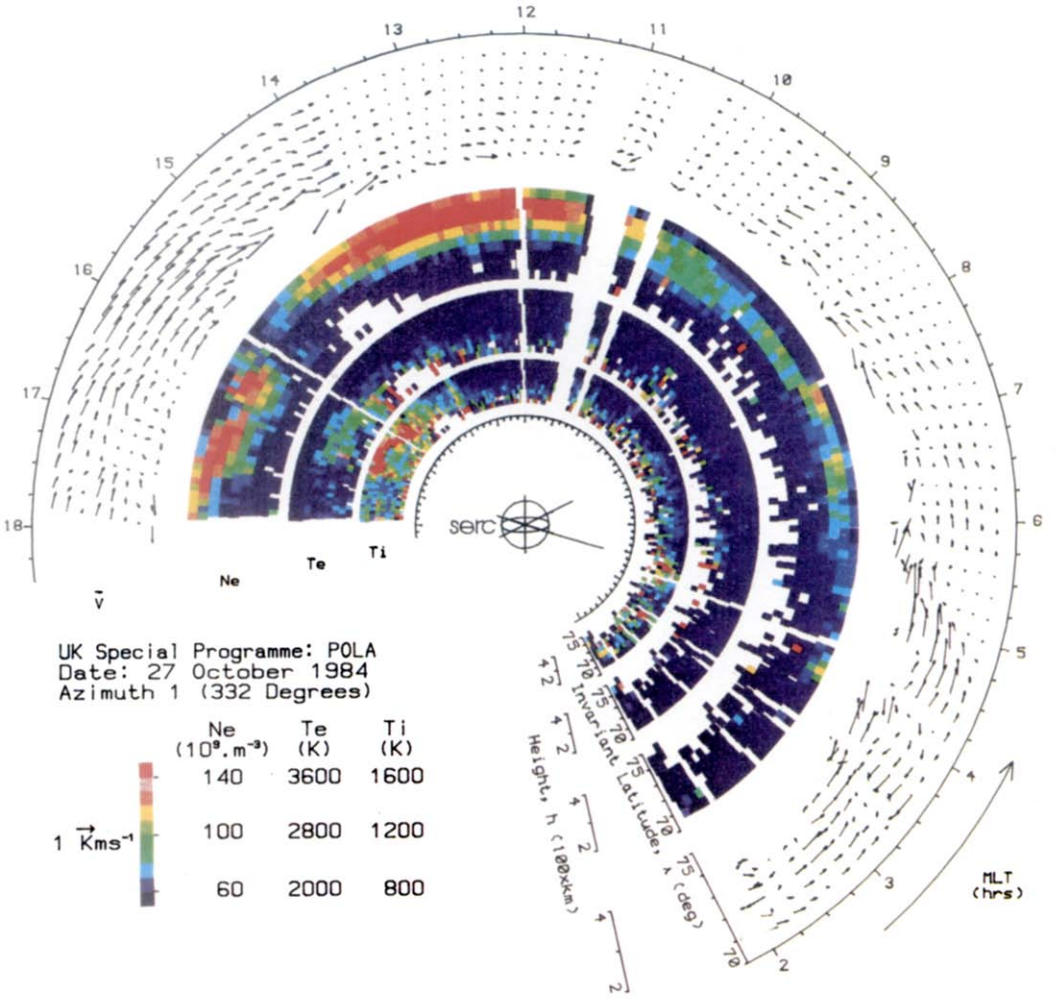

Fig. 7. As Fig. 5, but for 26–27 October 1984.

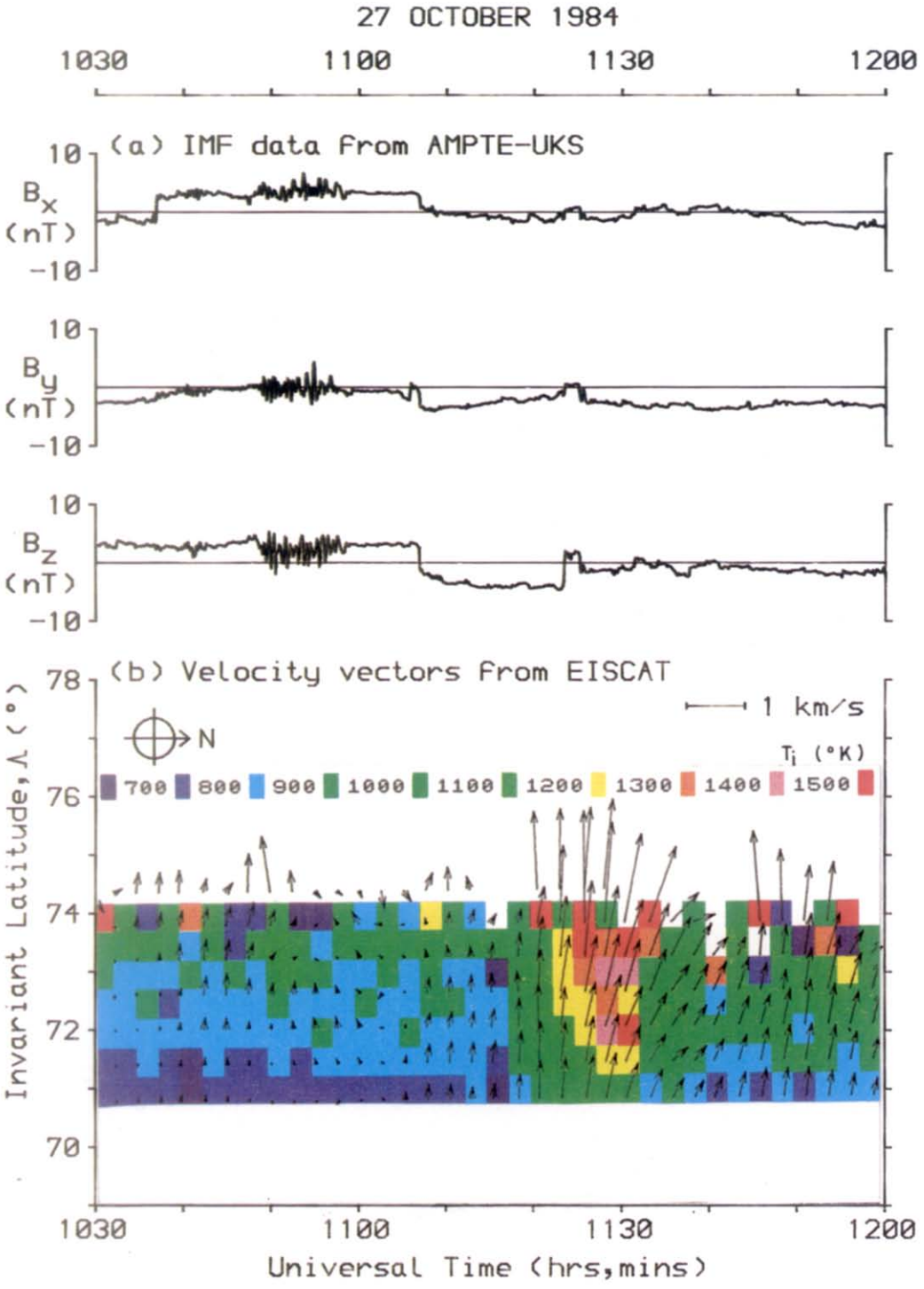

Fig. 9. As Fig. 2, but for the period 1030–1200 UT on 27 October, with 5 s resolution IMF data and colour-coded ion temperatures T_i superimposed on the velocity vectors. The IMF turned abruptly southward at 1107 UT and convection velocities and ion temperatures were strongly enhanced near 1120 UT.

if a throat exists: however, the strongly westward flows on 25 October at MLT > 1200 suggest that it does exist for this day and that it is in the morning sector.

The major differences between the convection observed on these three days occur in the afternoon sector (in the UT period 0930–1115, which corresponds roughly to 1200–1345 MLT). Prior to 1115 UT on 27 October, convection had been very sluggish for a 2–3 h period (see Figs. 4 and 7). For a southward IMF, strong westward flows would usually be expected during this period in the afternoon MLT sector, as was observed on 25 October (see Figs. 3 and 6). On 29 September, flows in this period were generally low also (see Figs. 2 and 5).

The differences in these flows in the afternoon sector can be explained in terms of the IMF data. On 27 October the period of slow convection corresponds to a 3 h period when the IMF was northward, sufficient time to allow the cross-cap potential to fall (WYGANT *et al.*, 1984) and cause a shrinking of the convection pattern to higher latitudes and a general reduction in convection speeds. During this period B_z exceeded 1 nT for a large part of the time, which has been quoted as the value required to shut off dayside merging for all B_y and cause it to occur at the cusps (MAEZAWA, 1976; BURKE et al., 1979). On 29 September at these times B_z was near zero and fluctuated around the zero value; the B_y value was negative (roughly −3 nT). The merging model of REIFF and BURCH (1985), which is an extrapolation from Dynamics Explorer observations (BURCH *et al.*, 1985), predicts that for small B_z and negative B_x only a dawn cell is observed when B_y is negative and only a dusk cell if B_y is positive (compare parts B and E of fig. 5 of REIFF and BURCH, 1985). This is true of either hemisphere, but the single cell is roughly circular in the north and crescent-shaped in the south, where it appears towards the centre of the polar cap (see also MOSES *et al.*, 1985). Thus the predictions of the merging model are consistent with the absence of the dusk cell before 1400 MLT on 29 September. The gradual reappearance of the dusk cell on 29 September (around 1115 UT) would therefore be due to the decrease in B_z (and simultaneous small increase in B_y). On 25 October, B_z was weakly southward during this period and, for positive B_y (roughly 3 nT), this is sufficient to drive relatively steady and strong convection.

5b. *Convection velocity variation with* B_z *component of the IMF*

Figure 8 shows scatter plots for two velocity components and the total velocity |V|, plotted against values of B_z measured 11 min previously. Both the velocity and the B_z data are averaged over periods of 2.5 min and data from all three days are used. The choice of a lag of 11 min is explained in Section 6a. Figure 8 demonstrates that the northward velocity $v_{\perp N}$ is generally small in the few cases when $B_z > 2$ nT, but a wide range of values is observed when $B_z < 0$. The same is true for the eastward component $v_{\perp E}$ and the magnitude of the flow |V| (Figs. 8b, c). In general, for $B_z < 0$ the flows are to the north and west, reflecting the MLT range of these mainly afternoon sector sub-auroral observations. A correlation of the flow speeds with B_z is apparent for $B_z < 0$, even in these plots which cover a range of MLT and B_y. The range of velocities observed for $0 < B_z < 2$ nT is larger than for $B_z > 2$ nT, consistent with the effect of geomagnetic flux which remains open after the IMF has turned northward and the consequent slow decay of the convection pattern, and possibly also the controlling influence of the other IMF components when B_z is small.

6. POSSIBLE CONVECTION RESPONSES TO ABRUPT CHANGES IN THE IMF

In this section the AMPTE-UKS magnetometer and EISCAT data sets are surveyed with a view to finding convection responses to changes in the IMF. This work can only identify changes which could have resulted from a given IMF change: to prove that the responses are the consequence of a given IMF change would require the statistical analysis of considerably more data than are available. The present study does give much information about IMF–ionosphere interactions, however, if the assumption about cause and effect is valid.

6a. *Southward turning of the IMF on 27 October*

The most dramatic effect seen in the whole three days' observations is at the end of the period of sluggish convection on 27 October, near 1115 UT, when a sudden increase in convection flows was observed (Fig. 7). This increase followed several minutes after the period of northward IMF had ended in an abrupt southward turning of the IMF. This event is shown with higher time resolution in Fig. 9. Roughly 10 min after the IMF turned southward at the UKS at 1107 UT, the velocities observed by EISCAT increased, with an almost simultaneous increase in ion temperature, presumably due to an increased ion–neutral frictional heating rate. An electron temperature increase was subsequently observed while the ions were cooling (RISHBETH *et al.*, 1985), which is thought to reflect ion–electron collisional heating and which may cause part of the drop in T_i. However, most

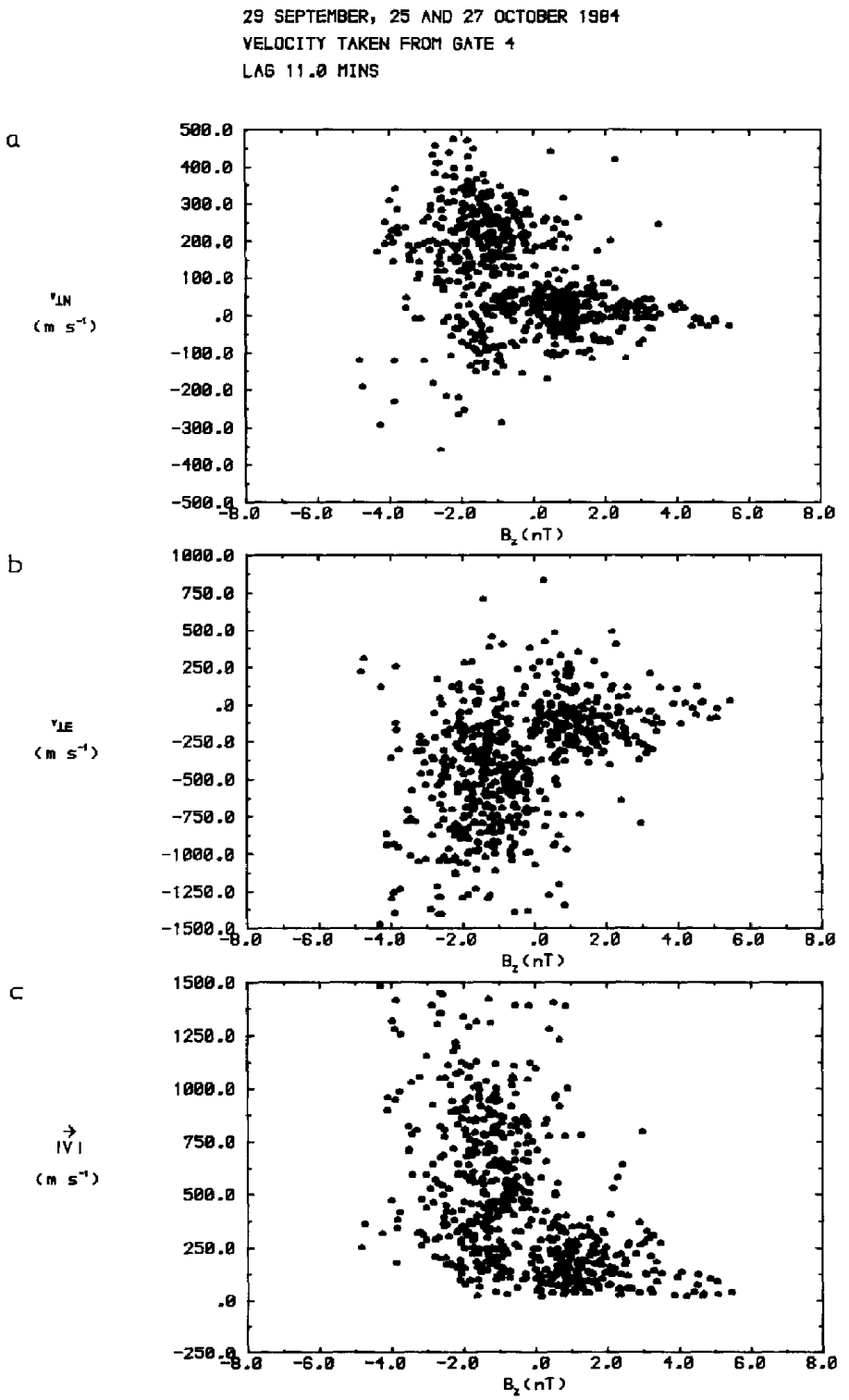

Fig.8. Scatter plots of (a) northward velocity $v_{\perp N}$, (b) eastward velocity $v_{\perp E}$ and (c) the magnitude of the velocity |V| as a function of B_z measured 11 min previously for the observations on all three days. The data are averaged over periods of 2.5 min.

of the drop occurred because the frictional heating decreased as the neutrals were accelerated by the ions. Careful inspection of Fig. 9 shows that after the initial increase in ion velocity around 1120 UT, there is a decrease which may be a response to the increase in B_z at 1125 UT (although it remains mainly negative after a brief positive excursion).

To quantify the lag between the change in B_z and the apparent response of the velocities, a standard cross-correlation analysis was carried out for a 1 h period about the southward turning (1045–1145 UT). The results are shown in the correlogram given in Figure 10. The correlation coefficient r is plotted as a function of lag τ for correlations between B_z and the northward and eastward components ($v_{\perp N}$ and $v_{\perp E}$, respectively) and the magnitude of the velocity ($|\mathbf{V}|$). The sense of τ adopted is such that a negative τ corresponds to the EISCAT-observed velocities lagging behind the IMF. For negative τ, good correlations are observed (r greater than 0.9 and the significance level exceeding 99%) in all three cases. Correlations are negative for $v_{\perp N}$ and $|\mathbf{V}|$, as they increase when the IMF turns southward (B_z decreases), but positive for $v_{\perp E}$ (i.e. westward flows increase). Curve-fitting shows that the peak correlation is at a lag of 11 ± 1 min for $v_{\perp E}$, but at a longer lag, 20 ± 1 min, for $v_{\perp N}$; the lag

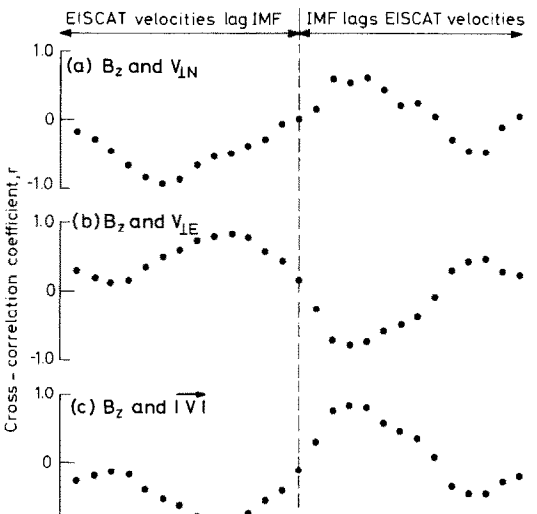

Fig. 10. Correlation coefficients of EISCAT convection velocities with the B_z component of the IMF as a function of lag, for (a) northward velocity $v_{\perp N}$, (b) eastward velocity $v_{\perp E}$ and (c) the magnitude of the velocity $|\mathbf{V}|$. Correlations are done for data in a 1 h period (1045–1145 UT) around the southward turning of the IMF shown in Fig. 9.

for $|\mathbf{V}|$ is as for $v_{\perp E}$, because $v_{\perp E}$ is by far the larger component. Note the width of the peaks in r, revealing large persistence in the data series. Figure 10 shows that if the IMF southward turning caused the increase in flow speeds, then the lag is 11 ± 1 min. However, the quality of the correlation does not confirm that the convection increase is a response to that IMF change. This point is underlined by the correlation coefficients for positive τ, where equally good and significant correlations were obtained at $\tau = 8$ min. These apparent correlations can be explained by looking at Fig. 9, and arise from the increase in B_z at 1125 UT (hence r has the opposite sense to the values for negative τ). It is not believed that this B_z change is a result of any cause and effect mechanism: rather, it is thought that, by chance, the IMF turned slightly back towards northward 19 min after the southward turning, so it is still possible that the correlation at $\tau = -11$ min arose also by chance. Proof that the two are related would require study of an extremely large period of joint observations containing a large number of southward turning events to give good statistics. The data from the ion experiment on UKS shows that the solar wind speed and density remain relatively constant throughout this period, only a very small decrease in solar wind density being observed while the IMF is most strongly southward (1107–1125 UT). Hence the convection change could not be a response to a change in solar wind pressure.

As discussed by Rishbeth *et al.* (1985), the 11 min lag of this apparent response is interesting. From the observed solar wind speed of 460 km s^{-1}, it is estimated that the IMF change would have impinged upon the dayside magnetopause 4 ± 1 min later, allowing for the slowing effect of the Earth's bow shock. A further delay of 2 ± 1 min is expected to allow for the field-aligned Alfvén wave propagation time from the dayside magnetopause to the cleft ionosphere. Hence the ionospheric response seen by EISCAT is observed 5 ± 3 min after the effect of opening geomagnetic field lines is first expected in the cleft region. This delay is similar to that reported in the past by Nishida (1968), McPherron and Manka (1985) and Clauer and Kamide (1985) from ground-based magnetometer studies and by Horwitz and Akasofu (1977) for the motion of dayside auroral forms. The POLAR field of view is near 1400 MLT at the time of the southward turning and Lockwood *et al.* (1986) have found that the convection enhancement appears to propagate eastward over the field of view with a speed of about 1 km s^{-1}. This speed is consistent with a delay of 5 min for the effect to propagate from the region where field lines first become open, in the cleft region, and with the rate at which geomagnetic flux can merge

with the IMF at the dayside magnetopause following the southward turning.

6b. *Sector boundary crossing on 27 October*

Another interesting event occurs at 1238 UT on 27 October, when an IMF sector boundary passes over the UKS, giving a change in sign of both B_x and B_y. This event is shown in greater detail in Fig. 11a and the simultaneous EISCAT velocity vectors are plotted in Fig. 11b. During this period B_z remained negative and approximately constant. No major change in the convection velocities was observed following the sector boundary crossing: however, the flow increased in magnitude and swung to almost due west (from north of west) at 1250 UT. It is interesting to note that, if this is a genuine response, the lag is very similar to that for the southward turning event described in Section 6a and to the delay for B_y effects in the cusp region reported by CLAUER and BANKS (1986). These delays are thought to have a similar origin to the lag associated with the southward turning, as explained by LOCKWOOD *et al.* (1986). However, there is an important difference: in this case it is necessary that sufficient flux is connected to the IMF before the B_y component can exert a magnetic tension effect, even in the cusp, whereas LOCKWOOD *et al.* (1986) explain the southward turning delay as an expansion time to a region outside the cusp. Simple models of the effect of B_y on the pattern of convection predict that the dusk cell observed here should turn from crescent-

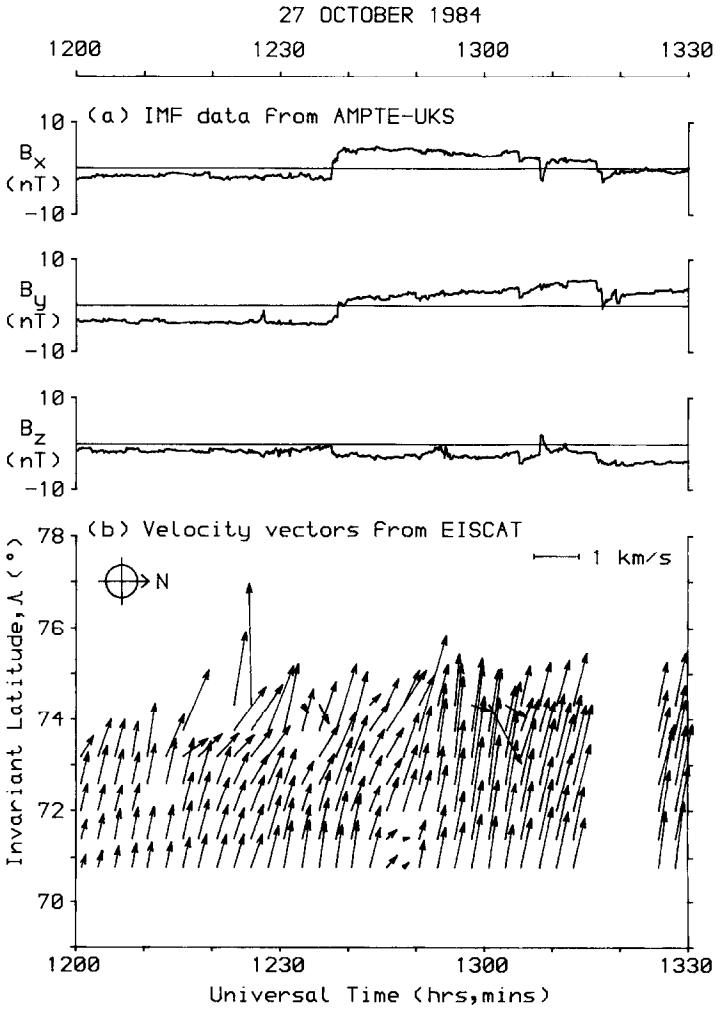

Fig. 11. As Fig. 2, but for the period 1200–1330 UT on 27 October, with 5 s resolution IMF data. An IMF sector boundary crossed UKS at 1238 UT.

shaped to circular as B_y turns positive. This seems to be at variance with the decrease in northward flow and the increase in flow magnitude observed here.

7. SHORT LIVED, RAPID FLOW BURSTS SEEN BY EISCAT

The final feature of the observations to be discussed here is the occurrence of bursts of rapid poleward flow (here called 'flow bursts') in the dayside morning sector. Figure 12 shows data from range gates 3–5 (corresponding to invariant latitudes 72.0°, 72.6° and 73.2°) obtained on 27 October. Here, 2 min integrated line-of-sight velocities are plotted separately for the two azimuths at each gate. It can be seen that the background flow was small during this period (0550–0750 UT); the observations were made in the pre-noon interval of low zonal flows between the two convection cells, i.e. the throat. Three intervals of perturbed flow are seen in this data, near 0610, 0640 and 0740 UT (add ~2.5 h for MLT). These intervals

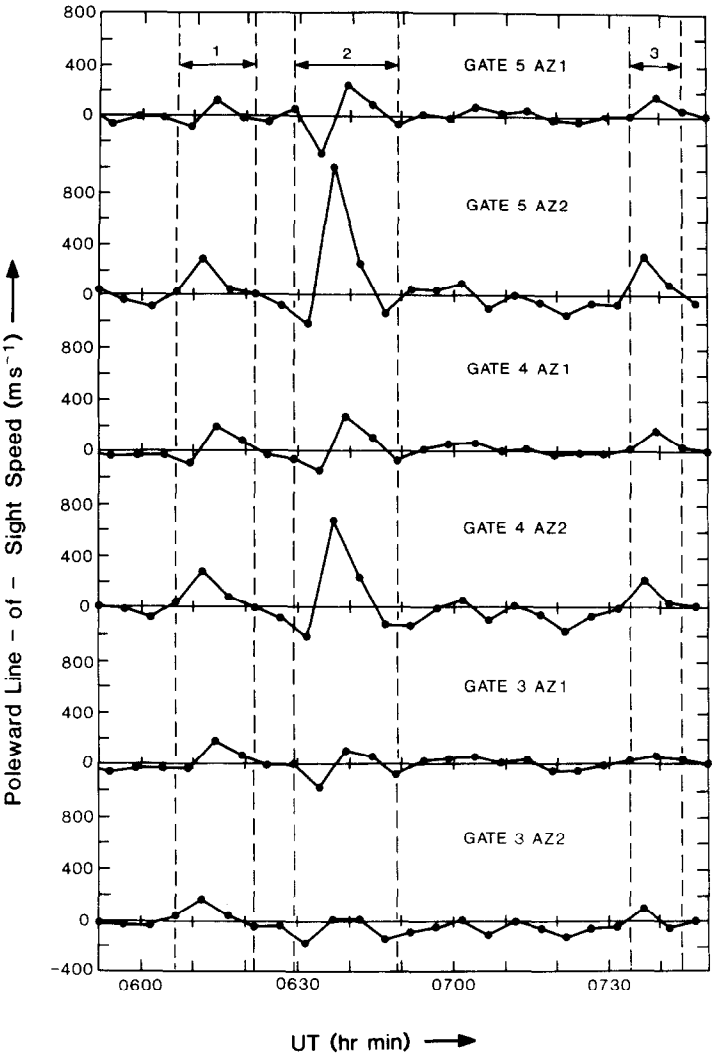

Fig. 12. Flow burst events seen on 27 October (labelled 1, 2 and 3). The line-of-sight velocities (positive values being poleward) are plotted as a function of UT for azimuths 332° (AZ 1) and 356° (AZ 2) for range gates 3–5.

last for 10–20 min each, but the main flow perturbation, involving a burst of poleward directed flow at speeds of up to ~ 1 km s^{-1}, is short lived and is observed for one 2 min integration period only in each case. Analysis of these data with 15 s integration periods shows great consistency from one data point to the next and a clear peak in poleward flow of ~ 2 km s^{-1}, and strongly suggests that the poleward flow burst is part of a twin vortex flow pattern (TODD *et al.*, 1986). Bursts of poleward flow have been predicted at the centre of the twin vortex flow pattern, which is the expected ionospheric signature of flux transfer events (FTEs) on the magnetopause (SOUTHWOOD, 1985; GOERTZ *et al.*, 1985).

From the short lived nature of the events, the fact that the main perturbation is seen in only one beam (the beams are separated in magnetic longitude by ~ 300 km for gate 5), and from the clear amplitude variations seen in Fig. 12 over a latitudinal range of only ~ 150 km (the separation of the centres of gates 3 and 5), it is clear that the flow perturbation has spatial scales of only ~ 200 km. This is similar to that expected for FTEs, considering their size at the magnetopause (SAUNDERS *et al.*, 1984) and magnetic flux conservation (COWLEY, 1984).

Poleward-directed flow bursts in the dayside high-latitude ionosphere have also been reported by VAN EYKEN *et al.* (1984), using other EISCAT-POLAR data, and by GOERTZ *et al.* (1985) and SOFKO *et al.* (1985), using data from the STARE radar. These are likely to be related to the 'pulsed' boundary layer which has been discussed either in terms of a reconnection-associated FTE phenomenon (e.g. COWLEY, 1982; PASCHMANN *et al.*, 1982) or in terms of 'impulsive penetration' of magnetosheath plasma onto closed field lines (LUNDIN, 1984). Both theories result in the expectation that impulsive structures will form in the region just equatorward of the polar cap boundary and that a small, twin vortex flow pattern will exist briefly (for a few minutes) in the ionosphere. However, for the impulsive penetration theory the strong flow at the centre of the pattern will be equatorward, not poleward as in the FTE theory (HEIKKILA, 1982; COWLEY, 1986).

The importance of the observations presented in this paper is that the main, central flow perturbation is poleward, consistent with the expectations based upon impulsive reconnection and FTEs, but not with the impulsive penetration picture. Similar conclusions were reached by GOERTZ *et al.* (1985).

8. CONCLUSIONS

The EISCAT and AMPTE observations here presented exploit a unique opportunity to study the response of high-latitude plasma convection to changes in the IMF. The data reveal the controlling influence of B_z in that if B_z is positive for a sufficiently long period of time, convection at the sub-auroral latitudes observed by EISCAT virtually disappears. However, when B_z is near zero the other two components of the IMF can determine the convection pattern. In these observations with negative B_x, a dusk cell was not observed when B_y was negative. A stagnation region was observed near dusk at $\Lambda > 72.0^\circ$ on the two days when B_y was strongly positive, but not on the one day for which it was near zero.

The observations also illustrate how the plasma convection pattern can determine the distribution of plasma density in the high-latitude ionosphere. This is the case for the observations made in October, when features like the mid-latitude trough (seen at high latitudes in the afternoon sector) and the morning–afternoon asymmetry in densities are apparent. In contrast, one month earlier solar photoionization dominates and the convection pattern is not such a major factor.

The unprecedented time resolution of the EISCAT data and the near-Earth location of AMPTE-UKS have allowed the lag between IMF changes and their apparent ionospheric convection responses to be quantified for the first time. The determination of a lag of 11 ± 1 min has interesting implications for our understanding of how the onset of IMF–geomagnetic field merging establishes a new enhanced pattern of convection in the ionosphere and magnetosphere.

Lastly, bursts of rapid poleward flow seen in the morning sector are found to be in agreement with the predictions of a reconnection-based theory and not with a picture of impulsive penetration of magnetosheath plasma into closed field lines, supporting the idea that these are the ionospheric signatures of flux transfer events.

Acknowledgements—We thank the Director and staff of EISCAT for their help, Dr D. J. SOUTHWOOD for the provision of AMPTE-UKS magnetometer data and Dr W. A. C. MIER-JEDRZEJOWICZ for aid in magnetometer data processing. EISCAT is supported by the British SERC, French CNRS, West German MPG, Norwegian NAVF, Swedish NFR and Finnish SA. AMPTE is a collaborative project of NASA (USA), DFVLR and MPG of the F.R.G. and SERC of the U.K. P.R.S. was supported by an SERC grant.

REFERENCES

Bryant D. A., Krimigis S. M. and Haerendel G.	1985	*I.E.E. Trans. Geosci. Remote Sensing* **GE-23,** 177.
Burch J. L. and Reiff P. H.	1985	*Adv. Space Res.* **5**(4), 23.
Burch J. L., Reiff P. H., Menietti J. D., Heelis R. A., Hanson W. B., Shawhan S. D., Shelley E. G., Sugiura M., Weimer D. R. and Winningham J. D.	1985	*J. geophys. Res.* **90,** 1577.
Burke W. J., Kelley M. C., Sagalyn R. C., Smiddy M. and Lai S. T.	1979	*Geophys. Res. Lett.* **6,** 21.
Cauffman D. P. and Gurnett D. A.	1972	*Space Sci. Rev.* **13,** 369.
Clauer C. R. and Banks P. M.	1986	*J. geophys. Res.* **91,** 6959.
Clauer C. R. and Kamide Y.	1985	*J. geophys. Res.* **90,** 1343.
Clauer C. R., Banks P. M., Smith A. Q., Jørgensen T. S., Friis-Christensen E., Vennerstrom S., Wickwar V. B., Kelley J. D. and Doupnik J. R.	1984	*Geophys. Res. Lett.* **11,** 891.
Coates A. J., Bowles J. A., Gowen R. A., Hancock B. K., Johnstone A. D. and Kellock S. J.	1985	*I.E.E. Trans. Geosci. Remote Sensing* **GE-23,** 287.
Cowley S. W. H.	1980	*The Physical Basis of the Ionosphere in the Solar–Terrestrial System*, AGARD Conference Proceedings, 295, p. 4-1.
Cowley S. W. H.	1981	*Planet. Space Sci.* **29,** 79.
Cowley S. W. H.	1982	*Rev. Geophys. Space Phys.* **20,** 531.
Cowley S. W. H.	1984	*Magnetic Reconnection in Space and Laboratory Plasmas*, A.G.U. Geophysical Monograph No. 30, p. 375.
Cowley S. W. H.	1986	*J. Geomagn. Geoelect.* (in press).
Evans J. V., Holt J. M., Oliver W. L. and Wand R. H.	1983	*J. geophys. Res.* **88,** 7769.
van Eyken A. P., Rishbeth H., Willis D. M. and Cowley S. W. H.	1984	*J. atmos. terr. Phys.* **46,** 635.
Fairfield D. H.	1977	*Rev. Geophys. Space Phys.* **15,** 285.
Farmer A. D., Lockwood M., Horne R. B., Bromage B. J. I. and Freeman K. S. C.	1984	*J. atmos. terr. Phys.* **46,** 473.
Friis-Christensen E., Kamide Y., Richmond A. D. and Matsushita S.	1985	*J. geophys. Res.* **90,** 1325.
Goertz C. K., Nielsen E., Korth A., Glassmeier K. H., Haldoupis C., Hoeg P. and Hayward D.	1985	*J. geophys. Res.* **90,** 4069.
Haerendel G., Paschmann G., Sckopke N., Rosenbauer H. and Hedgecock P. C.	1978	*J. geophys. Res.* **83,** 3195.
Heelis R. A.	1982	*Rev. Geophys. Space Phys.* **20,** 567.
Heelis R. A.	1984	*J. geophys. Res.* **89,** 2873.
Heelis R. A.	1986	*Morphology and Dynamics of the Polar Cusp.* D. Reidel, Dordrecht.
Heelis R. A. and Hanson W. B.	1980	*J. geophys. Res.* **85,** 1995.
Heelis R. A. and Reiff P. H.	1985	*Adv. Space Res.* **5**(4), 349.
Heelis R. A., Foster J. C., de la Beaujardiere O. and Holt J.	1983	*J. geophys. Res.* **88,** 10111.
Heikkila W. J.	1982	*Geophys. Res. Lett.* **9,** 159.
Heppner J.P.	1972	*J. geophys. Res.* **77,** 4877.
Horwitz J. L. and Akasofu S.-I.	1977	*J. geophys. Res.* **82,** 2723.
Jørgensen T. S., Friis-Christensen E. and Wilhjelm J.	1972	*J. geophys. Res.* **77,** 1976.
Jørgensen T. S., Friis-Christensen E., Wickwar V. B., Kelly J. D., Clauer C. R. and Banks P. M.	1984	*Geophys. Res. Lett.* **11,** 887.
Lockwood M., Farmer A. D., Opgenoorth H. J. and Crothers S. R.	1984	*J. atmos. terr. Phys.* **46,** 489.
Lockwood M., van Eyken A. P., Bromage B. J. I., Willis D. M. and Cowley S. W. H.	1986	*Geophys. Res. Lett.* **13,** 72.
Lundin R.	1984	*Planet Space Sci.* **32,** 757.

MAEZAWA K.	1976	*J. geophys. Res.* **81,** 2289.
MCPHERRON R. L. and MANKA R. H.	1985	*J. geophys. Res.* **90,** 1175.
MOSES J. J., CROOKER N. U., GORNEY D. J. and SISCOE G. L.	1985	*J. geophys. Res.* **90,** 11078.
MOZER F. S.	1984	*Geophys. Res. Lett.* **11,** 135.
NISHIDA A.	1968	*J. geophys. Res.* **73,** 5549.
PASCHMANN G., HAERENDEL G., PAPAMASTORAKIS I., SCKOPKE N., BAME S. J., GOSLING J. T. and RUSSELL C. T.	1982	*J. geophys. Res.* **87,** 2159.
PRIMDAHL F., PRIMDAHL I. S. and SPANGSLEV F.	1980	*J. geophys. Res.* **85,** 33.
PRIMDAHL F., PRIMDAHL I. S. and SPANGSLEV F.	1981	*J. geophys. Res.* **86,** 875.
REIFF P. H.	1982	*J. geophys. Res.* **87,** 5976.
REIFF P. H. and BURCH J. L.	1985	*J. geophys. Res.* **90,** 1595.
REIFF P. H., SPIRO R. W. and HILL T. W.	1981	*J. geophys. Res.* **86,** 7639.
RISHBETH H., SMITH P. R., COWLEY S. W. H., WILLIS D. M., VAN EYKEN A. P., BROMAGE B. J. I. and CROTHERS S. R.	1985	*Nature* **318,** 451.
RUSSELL C. T. and ELPHIC R. C.	1978	*Space Sci. Rev.* **22,** 681.
SAUNDERS M. A., RUSSELL C. T. and SCKOPKE N.	1984	*Geophys. Res. Lett.* **11,** 131.
SHAH H. M., HALL D. S. and CHALONER C. P.	1985	*I.E.E. Trans. Geosci. Remote Sensing* **GE-23,** 293.
SOFKO G. J., KORTH A. and KREMSER G.	1985	*J. geophys. Res.* **90,** 1449.
SOUTHWOOD D. J.	1985	*Adv. Space Res.* **5**(4), 7.
SOUTHWOOD D. J., MIER-JEDRZEJOWICZ W. A. C. and RUSSELL C. T.	1985	*I.E.E. Trans. Geosci. Remote Sensing* **GE-23,** 301.
TODD H., BROMAGE B. J. I., COWLEY S. W. H., LOCKWOOD M., VAN EYKEN A. P. and WILLIS D. M.	1986	*Geophys. Res. Lett.* (in press).
WYGANT J. R., TORBERT R. B. and MOZER F. S.	1983	*J. geophys. Res.* **88,** 5727.
ZANETTI L. J., POTEMRA T. A., IIJIMA T., BAUMJOHANN W. and BYTHROW P. F.	1984	*J. geophys. Res.* **89,** 7453.

APPENDIX: ERRORS IN THE VELOCITY VECTOR DERIVED FROM THE UK-POLAR BEAM-SWINGING EXPERIMENT

This Appendix discusses the errors that occur in velocity measurements in a beam-swinging experiment such as UK-POLAR, in which velocity vectors are derived by combining the line-of-sight velocities V_1, V_2 measured in two beam directions at geographic azimuths $\theta-\psi$, $\theta+\psi$, separated by an angle 2ψ (Fig. 13). The discussion refers to the velocities in the plane of the radar beams, slightly inclined to the plane normal to the geomagnetic field, in which the results are eventually presented. This inclination, amounting to only a few degrees, introduces small corrections (no more than a few per cent) which will here be ignored.

For the UK-POLAR experiment $\theta = 344°$, $\psi = 12°$. The basic assumption is therefore that the velocity vector **V** is sufficiently slowly-varying, in both space and time, that it may be assumed to be the same at both points of measurement (P_1 and P_2) and at their midpoint, and to vary linearly during a beam-swinging period. A further assumption, necessary in the UK-POLAR experiment, is that one component of **V** (i.e. the component parallel to the magnetic field) can be neglected. Then the vector **V** at the midpoint has 'line-of-sight' and 'perpendicular' components, as seen from the transmitter, given by

$$V_L = (V_1+V_2)/2\cos\psi, \tag{1}$$

$$V_P = (V_1-V_2)/2\sin\psi. \tag{2}$$

If the vector **V** has azimuth A with respect to the line-of-sight direction, and magnitude W, then

$$V_2+V_1 = 2W\cos A\cos\psi, \tag{3}$$

$$V_2-V_1 = 2W\sin A\sin\psi. \tag{4}$$

Hence,

$$\tan A = V_P/V_L = \frac{V_2-V_1}{V_2+V_1}\cot\psi, \tag{5}$$

$$W^2 = V_L^2+V_P^2 = \frac{V_1^2+V_2^2-2V_1V_2\cos 2\psi}{\sin^2 2\psi}. \tag{6}$$

Furthermore,

$$W^2 = \frac{(V_2+V_1)^2}{4\cos^2\psi}+\frac{(V_2-V_1)^2}{4\sin^2\psi}. \tag{7}$$

Figure 13 is drawn to resemble the layout of the actual 'POLAR' experiment and the vectors are drawn such that V_1, V_2, V_L and V_P are all positive, using the radar convention that approach velocity is positive and recession velocity is negative.

The random errors in V_1 and V_2 are assumed to be independent and to have the same standard error ΔV. Then the resulting standard error of the magnitude W is given by

$$\Delta W = \sqrt{\{(\partial W/\partial V_1)^2+(\partial W/\partial V_2)^2\}}\Delta V. \tag{8}$$

The standard error in azimuth is given by

$$\Delta A = \sqrt{\{(\partial A/\partial V_1)^2+(\partial A/\partial V_2)^2\}}\Delta V. \tag{9}$$

On differentiating (5),

$$\frac{\partial A}{\partial V_1}\sec^2 A\tan\psi = \frac{-2V_2}{(V_2+V_1)^2}, \tag{10}$$

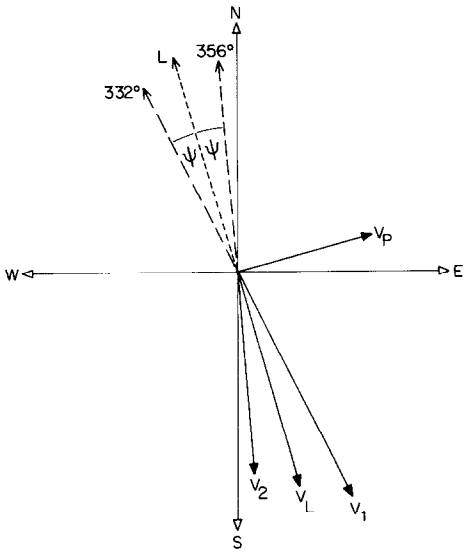

Fig. 13. Velocity vectors for UK-POLAR. The thin perpendicular axes are the geomagnetic cardinal directions (North at top); the dotted arrow L shows the direction θ of the L-shell meridian 334°; the beam directions 332° and 356° are shown by dashed arrows. V_1 and V_2 are the observed components of the plasma velocity, of which the line-of-sight and perpendicular components are V_L and V_P.

$$\frac{\partial A}{\partial V_2}\sec^2 A \tan\psi = \frac{2V_1}{(V_2+V_1)^2}, \tag{11}$$

from which the standard error in A is found to be

$$\Delta A = (\Delta V/W)\{1+\cos 2A \cos 2\psi\}^{1/2}/\sin 2\psi. \tag{12}$$

This shows that the azimuthal error ΔA is inversely proportional to the magnitude W, as might be expected, and depends on direction.

For the standard error in the magnitude W, differentiating (6),

$$2W\frac{\partial W}{\partial V_1} = \frac{V_2+V_1}{2\cos^2\psi} - \frac{V_2-V_1}{2\sin^2\psi}, \tag{13}$$

$$2W\frac{\partial W}{\partial V_2} = \frac{V_2+V_1}{2\cos^2\psi} + \frac{V_2-V_1}{2\sin^2\psi}, \tag{14}$$

from which the standard error in the magnitude W is found to be

$$\Delta W = \Delta V\{1-\cos 2A \cos 2\psi\}^{1/2}/\sin 2\psi, \tag{15}$$

which also depends on direction. It is convenient to define functions $F_W(A)$, $F_A(A)$ to describe the directional dependence of the errors such that

$$\Delta W = F_W(A)\cdot\Delta V, \tag{16}$$

$$\Delta A = F_A(A)\cdot(\Delta V/W). \tag{17}$$

Table 2 gives values of $F_W(A)$ and $F_A(A)$ for various azimuths between 0° and 90°, including one beam direction ($A = 12°$) and one direction perpendicular to a beam ($A = 78°$). The values for other ranges of A are easily obtained by symmetry. Table 2 shows that, for a given ratio $(\Delta V/W)$, the azimuthal error varies by a factor of 4.7 over the whole range of azimuths. Also tabulated are numerical values of the standard errors, taking $\Delta V = 25$ m s^{-1}, which is typical of the UK-POLAR data. The two values of ΔA correspond to $W = 100$ m s^{-1} and $W = 500$ m s^{-1}, which represent 'quieter' and 'more active' parts of the flow pattern. The error ΔA is greatest if $A = 0°$ or 180° (i.e. the velocity vector is parallel or anti-parallel to the mean pointing direction θ) and smallest if $A = \pm 90°$ (i.e. the velocity vector is perpendicular to the mean pointing direction). The standard error ΔW in the magnitude W varies in an opposite fashion, being smallest in the mean pointing direction ($A = 0°$, 180°) and greatest in the perpendicular direction ($A = \pm 90°$).

It is well known that a beam-swinging experiment such as UK-POLAR, in which the angle 2ψ between the beam directions is quite small, gives a poor measurement of velocities perpendicular to the mean line-of-sight. In this case, the sum (V_2+V_1) is small and, as can be seen from equation (7), W depends mainly on the term with the small denominator $4\sin^2\psi$. This tendency is accentuated in the case of UK-POLAR by the fact that (magnetic) east–west velocities are usually larger than north–south velocities. Nevertheless, the westward and eastward flows recorded at various times in the UK-POLAR observations do have the appearance of being quite well organized, without large random errors (except in more distant gates). This gives confidence in the validity of the technique.

If, beside the random errors, there exist systematic errors v_1, v_2 in the measured components V_1, V_2, there will be sys-

Table 2. Numerical coefficients for errors in magnitude $F_W(A)$ and direction $F_A(A)$ as a function of azimuth A, where $A = 0°$ refers to the mean direction $\theta = 344°$ [see equations (16), (17)]

A (deg)	$F_W(A)$	$F_A(A)$	ΔW (m s^{-1})	$\Delta A(100)$ (deg)	$\Delta A(500)$ (deg)
0	0.72	3.40	18	49	10
12	1.00	3.33	25	48	10
30	1.81	2.97	45	43	9
45	2.46	2.46	62	35	7
60	2.97	1.81	74	26	5
78	3.33	1.00	83	14	3
90	3.40	0.72	85	10	2

The numerical values of ΔA and ΔW assume that $\Delta V = 25$ m s^{-1}. The columns $\Delta A(100)$ and $\Delta A(500)$ are computed for $W = 100$ m s^{-1} and $W = 500$ m s^{-1}.

tematic errors w, a in magnitude and direction of the derived vector velocity. These are given by

$$w = (\partial W/\partial V_1)v_1 + (\partial W/\partial V_2)v_2, \tag{18}$$

$$a = (\partial A/\partial V_1)v_1 + (\partial A/\partial V_2)v_2. \tag{19}$$

In the special case in which $v_1 = v_2 = v$, these simplify to

$$w = v \cos A \sec \psi, \tag{20}$$

$$a = -(v/W) \sin A \sec \psi. \tag{21}$$

These also vary with direction, but in a different way from the random errors as given by (12) and (15).